Scientific Research Publishing

Journal of Power and Energy Engineering, 2022, 10, 54-64
https://www.scirp.org/journal/jpee
ISSN Online: 2327-5901
ISSN Print: 2327-588X

Numerical Investigation on Residual Stress and Warping of Planar SOFC in Manufacturing

Xumeng Zhang*, Jianguo Zhu, Wenlong Li

Faculty of Civil Engineering and Mechanics, Jiangsu University, Zhenjiang, China
Email: *zhangxumeng202112@163.com

How to cite this paper: Zhang, X.M., Zhu, J.G. and Li, W L. (2022) Numerical Investigation on Residual Stress and Warping of Planar SOFC in Manufacturing. *Journal of Power and Energy Engineering*, **10**, 54-64.
https://doi.org/10.4236/jpee.2022.105004

Received: May 5, 2022
Accepted: May 28, 2022
Published: May 31, 2022

Abstract

Residual thermal stresses and warping of the anode-supported planar solid oxide fuel cell (SOFC) were estimated numerically. A 3D finite element (FE) model with viscoelastic constitutive equations was established to calculate the residual stress and warping for the cell. In the fabrication of the cells, some mechanical restriction was employed during the high-temperature treatment followed by a cooling stage in order to prevent the button cell from warping, and then from these specific boundaries and loading conditions, a FE simulation was used to calculate the distribution of the internal stresses in the cell. The results indicate that the concentration of compressive stress appears in the electrolyte layer, and that could cause interfacial micro-cracks or even cohesive failure. Furthermore, from the numerical study, the annealing time (or continuous cooling) is related to the residual stress in the material due to creeping. The compressive stress in the electrolyte layer can be reduced significantly by increasing the cooling time. Therefore, it is possible to optimize the annealing time in order to make the SOFCs flat and have less residual stress, improving the mechanical durability.

Keywords

Solid Oxide Fuel Cell, Residual Stress, Warping; Numerical Simulation

1. Introduction

A solid oxide fuel cell (SOFC) is a device that converts chemical energy into electrical energy continuously by an electrochemical reaction. It is an attractive electricity generation device due to its high electrical energy conversion efficiency, low environmental pollution, and fuel flexibility [1]. There are two main kinds of SOFCs in design, tubular and planar. The planar SOFC is widely studied for its easy manufacturing and high power density. Usually, the single SOFC will

be piled up in series to provide a higher working power. Commercially, the SOFC stack is required to have at least 40000 h operation time with a power loss of less than 10% [2].

A single planar SOFC mainly consists of an electrolyte, anode, and cathode. Generally, the anode-supported cells are fabricated by co-firing a thin electrolyte on the thick (typically by 20 - 100 times) anode substrate at 1300˚C. Ni/YSZ and YSZ are used for the anode and the electrolyte, respectively. The thermal expansion coefficient (TEC) of Ni/YSZ is higher than that of YSZ, as a result, large residual stress will be induced in the cell at the end of manufacturing. The residual stress may induce large deformation and subsequently cause problems in the fixation of the cells in the SOFC stack. Commercially, SOFCs are mechanically restricted by high pressure during fabrication, so that the final SOFCs are flat to make the fixation of the flattened cells in the SOFC stack easier. However, the residual stress may initiate micro-cracks in the brittle SOFC materials resulting in fatal damage to the entire stack under thermal cycles [3]. As a result, mechanical failure of SOFCs often happens to shorten the service life.

Residual stresses in SOFC have been measured by X-ray diffraction (XRD) using the standard $\sin^2\psi$ method [4] [5] [6] [7]. For the linear elastic deformation of the material, the stress responsible for the lattice strain in the polycrystalline 8YSZ was evaluated by following the shift of a Bragg reflection for different incident X-ray angles at room temperature. The residual stresses were also evaluated from the curvature measurement of half-cells at room temperature integrated with a computational model using classical laminate theory [6] [8] [9] [10]. Generally, the stress analysis is complicated using the elastic-plastic constitutive relations because there are so many unknowns for the materials at super-high temperatures [11] [12]. For the prediction of the stress evolution of SOFCs during manufacturing and operation, there are many finite element (FE) analyses taking into account of kinds of aspects, such as residual stresses of a microstructure in the multilayered materials [13] [14], creep strain and strain rate [12] [14], transient creep [15] [16] and creeping behavior in the substrate and film [12]. Other literature shows the temperature profiles in the SOFCs using the coupled thermo-electrochemical model in the simulation [17] [18] [19]. It is essential to estimate the residual stresses of SOFC during manufacturing because the residual stresses could result in irreversible deformation. Otherwise, the poor gas tightness and electrical contact during the SOFC assembling could greatly degrade the performance of the SOFC stack. However, there are few studies focusing on the warping and residual stresses for the SOFCs during manufacturing.

The aim of the present work is to minimize the residual stresses and warping in the planar SOFC by optimizing the fabrication process. In this research, a 3D FE structure model was established and viscoelastic modeling was used as governing equations. The residual stresses and warping of the cell were calculated. From the numerical studies, the fabrication process was optimized so that the

residual stresses and warping of the final sample at the end of the fabrication will be reduced significantly.

2. Numerical Simulation

2.1. SOFC Sample

The anode-supported cell was manufactured in the H_2-Bank Co., Ltd. in China. Cross-sectional morphology of the button SOFC was observed by scanning electron microscope (Hitachi, S4800/SU70). As can be seen in Figure 1 there are four layers in the button SOFC: cathode, barrier layer, electrolyte, and anode, and the thickness of each layer is 20 μm, 2 μm, 9 μm, and 460 μm, respectively. The microstructure image shows that the anode has a porous structure while the internal pattern of the electrolyte is very dense.

2.2. FEM Model

Our button half-cell model consists of a NiO-YSZ anode and a YSZ electrolyte. A quarter structural model was adopted due to the symmetry of the geometry. The structural model, boundary, and loading conditions are shown in Figure 2. The electrolyte has a thickness of 9 μm and the thickness of the anode is 460 μm in accordance with the dimension shown in Figure 1. The diameter of the specimen is 20 mm. The bottom boundary edge of the metallic frame was constrained in the *z*-direction ($U_z = 0$) to restrict the movement of the SOFC, and the X- and Y-symmetric boundary conditions were applied to the two cross-sections. The element type is C3D8R. The temperature field was applied to the total elements in the model and was assumed to be uniform over the sample. The thermal and mechanical properties used in the analysis are shown in Table 1.

Based on the generalized Hook's law, the constitutive relationship takes into account the thermal mismatch and creep deformation, which can be expressed as [12].

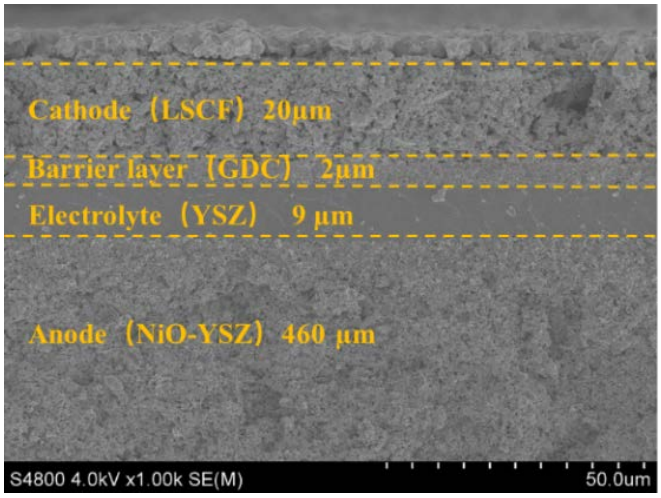

Figure 1. Cross-sectional morphology of the button SOFC by scanning electron microscope.

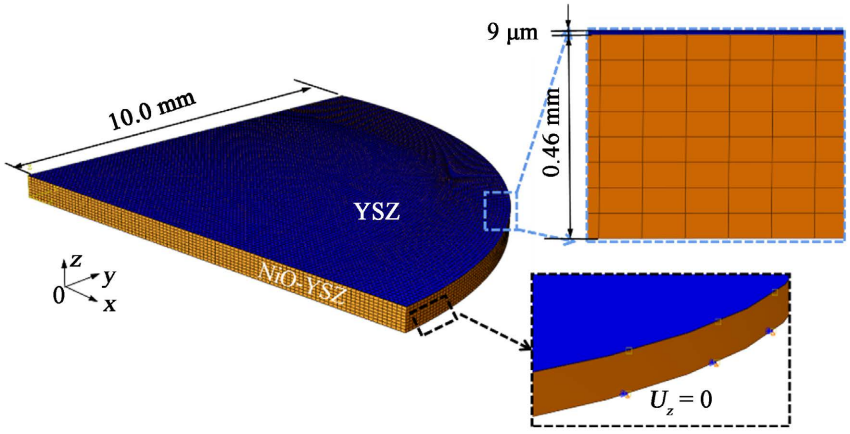

Figure 2. A finite element model of the NiO-YSZ/8YSZ button half-cell.

Table 1. Thermal and mechanical properties of YSZ and NiO-YSZ [20].

	Temperature (˚C)	20	200	400	600	800	1000
YSZ	E (GPa)	196.3	196.3	196.3	196.3	196.3	200
	ν	0.33	0.33	0.33	0.33	0.33	0.33
	α (10^{-6} K^{-1})	7.6	8.2	8.8	9.6	10.0	10.5
NiO-YSZ	E (GPa)	126.5	126.5	126.5	126.5	126.5	104
	ν	0.33	0.33	0.33	0.33	0.33	0.39
	α (10^{-6} K^{-1})	11.7	12.31	12.37	12.41	12.41	12.41

Table 2. Geometry and coefficients of YSZ and NiO-YSZ in the FEA [12].

	Thickness (μm)	A	n
YSZ	9	2.6×10^{-11}	1.7
NiO-YSZ	460	1.18×10^{-14}	1

$$\bar{\sigma} = E^* \left(\bar{\varepsilon} - \bar{\varepsilon}^{\theta} - \bar{\varepsilon}^{cr} \right), \tag{1}$$

where $\bar{\sigma}$ is the equivalent stress (or Von Mises stress), $\bar{\varepsilon}$ is the equivalent strain which is calculated in an equation of $\bar{\varepsilon} = \sqrt{\frac{2}{3}\boldsymbol{\varepsilon} : \boldsymbol{\varepsilon}}$, E^* is a coefficient which is related with the elastic modulus E and Poisson's ratio ν of the material and can be determined using the relation of the equivalent stress and strain, $\bar{\varepsilon}^{\theta} = \alpha \Delta\theta$ is the mismatch strain due to the change in temperature and α is the thermal expansion coefficient, $\bar{\varepsilon}^{cr}$ is the equivalent accumulated creep strain which is governed by the classical power-law creep model

$$\dot{\bar{\varepsilon}}^{cr} = A\bar{\sigma}^n, \tag{2}$$

where A is the creep constant and n is the stress exponent which are shown in Table 2. The simulation was carried out using the commercial finite element analysis (FEA) software Abaqus.

2.3. High-Temperature Deformation and Stresses

Firstly, the thermal-mechanical analysis during the fabrication of YSZ/NiO-YSZ double-layer structure was analyzed. Zero stress state was assumed in the materials by co-firing at the high temperature of 1350˚C in 4 hours, and the pressure (mechanical restriction) was applied uniformly on the sample during cooling down to room temperature. Figure 3 shows the *z*-displacement and distributions of the residual stress for the YSZ/NiO-YSZ double-layer structure with mechanical restriction of 0.21 MPa during cooling. Figure 3(a) shows that the maximum *z*-displacement is about 50 μm which indicates that the cell surface is almost flat under mechanical restriction after cooling. However, large compressive residual stress appears in the YSZ layer and the maximum value is about 1666 MPa, as shown in Figure 3(b).

3. Optimizing the Fabrication Process

The influence of the various external pressures on the deformation and the maximum residual stress in the SOFC cell was studied. As shown in Figure 4(a), the warping of the cell increases with the decreasing of the external pressure, and

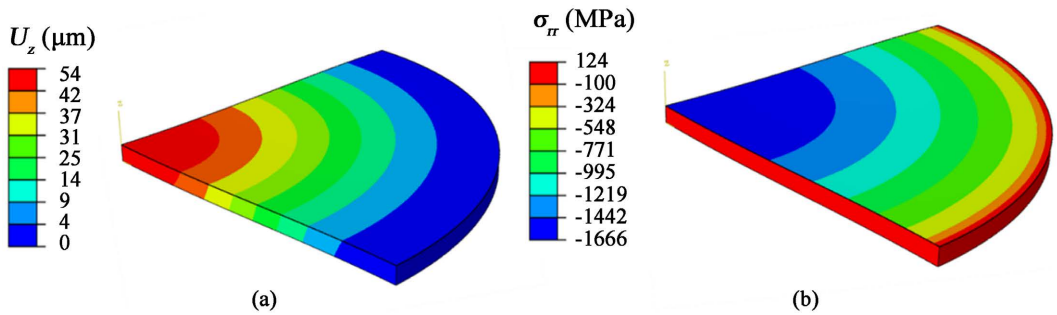

Figure 3. (a) Z-displacement and (b) residual stress distribution of the YSZ/NiO-YSZ double-layer SOFC under the mechanical restriction of 0.21 MPa after cooling.

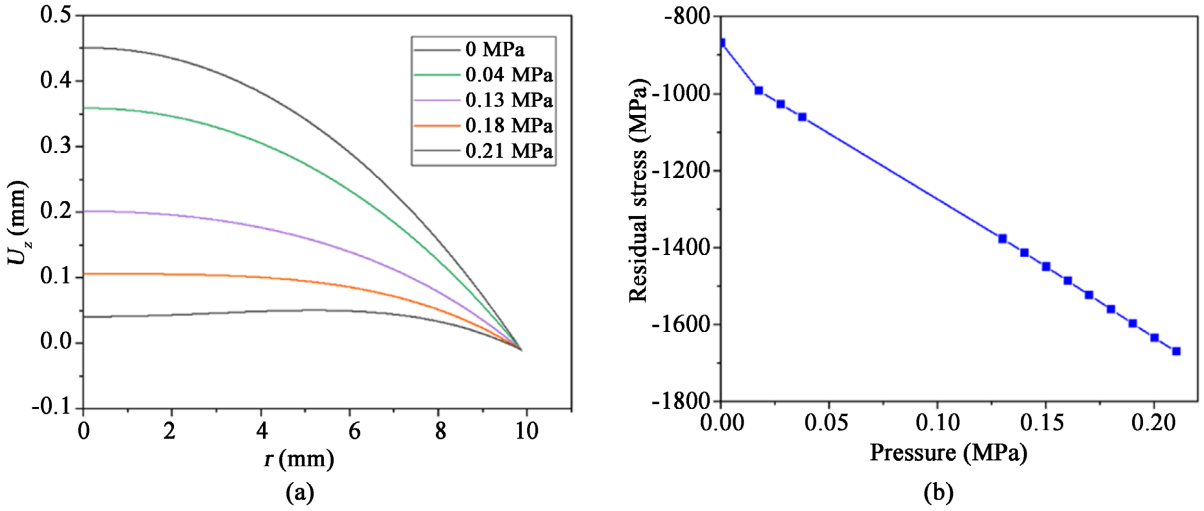

Figure 4. (a) Z-displacement in the radical direction under different pressures and (b) the maximum residual stress for YSZ as a function of external pressure.

the largest *z*-displacement reaches about 0.45 mm with the free of mechanical restriction. Moreover, Figure 4(b) shows that the residual stress in YSZ was calculated with different pressures, and the residual stress increases when the larger pressure is applied. The residual stress of YSZ is always in compressive status and the minimum value of the compressive stress is about 800 MPa. From these results, it is possible to obtain the small value of warpage or the small residual stresses for the SOFC cell by controlling the mechanical restriction during the cooling down process.

Secondly, two FE simulations were conducted for the flat YSZ/NiO-YSZ double-layer structure, respectively, under heating up to 1300˚C in 4 hours and under cooling down to room temperature in about 30 hours with no mechanical restriction. As shown in Figure 5(a) & Figure 5(b), it can be seen that the *z*-displacement is in the range of −75 - 0 μm and the associated radial stress is mainly in tensile stress status within 270 MPa when the YSZ/NiO-YSZ was heated from room temperature to 1300˚C. The results indicate that the YSZ/NiO-YSZ double layer material shows a small residual stress with the initial flat surface. When it cools down to room temperature, as shown in Figure 5(c) & Figure 5(d), the morphography shows a convex with the maximum *z*-displacement of 0.46 mm, and the distribution of the residual stress over the sample shows that the small tensile stress of about 100 MPa is located in the anode while the maximum compressive residual stress, 877 MPa, almost homogeneously appears in the YSZ plane. Compared with the results in Figure 3(b), the compressive stress was released by around 50% due to the warping when there is no constraint during cooling. These residual stresses are consistent with

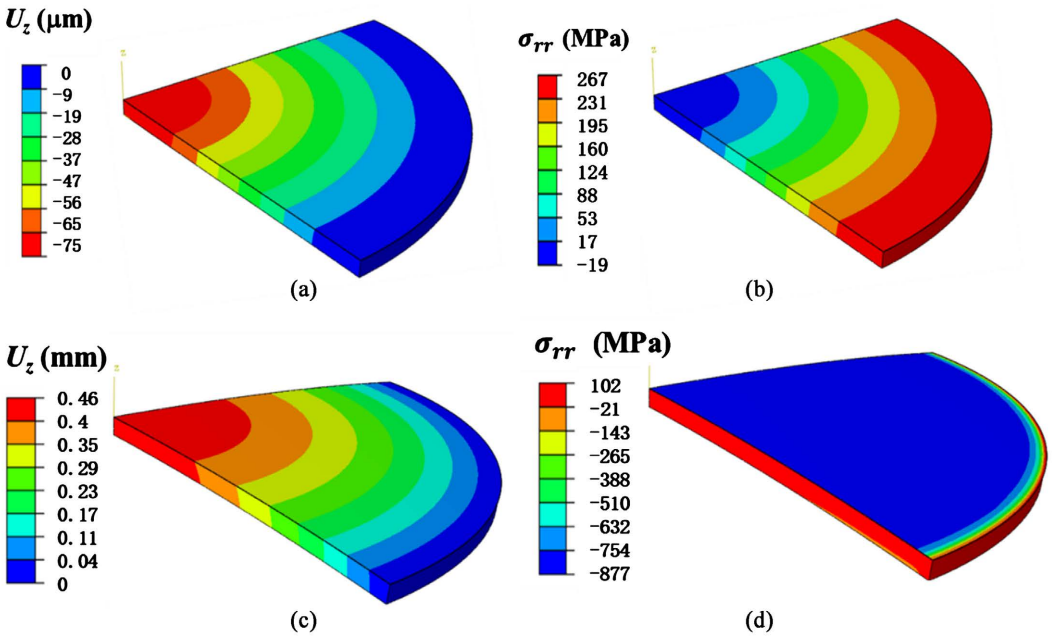

Figure 5. (a) *Z*-displacement and (b) radial stress distribution of YSZ/NiO-YSZ under heating up to 1300˚C; (c) *z*-displacement and (d) residual stress distribution in YSZ/NiO-YSZ during cooling down to room temperature. The two simulations are free of mechanical restrictions.

the previous report [3], which presented that the residual compressive stress in the electrolyte of the anode-support planar SOFC estimated using the X-ray diffraction method was around 650 MPa.

Thirdly, according to the analysis of creep curve of metal, stress relaxation and strain accumulation will occur with the increase of creep time under the condition of constant stress. In this study, the creep time of YSZ/NiO-YSZ double-layer structure without mechanical constraint was increased, that is, the cooling process time (cooling time) was increased to reduce the residual compressive stress of YSZ layer.

As shown in **Figure 6(a)**, stress relaxation occurs continuously with the increase of cooling time. The maximum residual stress of YSZ layer decreases from −884.14 MPa to −306.84 MPa, but the decreasing rate of residual stress gradually slows down. Meanwhile, as shown in **Figure 6(b)**, the deformation in the overall thickness direction of the sample gradually accumulates. As the distance between the deformation curves gradually decreases, it can be seen that the rate of deformation increase also gradually decreases. When the cooling time approaches 7 days, the overall residual stress and thickness direction change tend to be stable.

The creep strain during the cooling stage was recorded with the cooling time, as shown in **Figure 7(a)**. It shows that the creep strain increases nonlinearly with the cooling time. In addition, the creep strain rate was calculated, as shown in **Figure 7(b)**. The strain rate builds up to the maximum value in around 25 hours and then goes down quickly. It indicates that the materials creep fast and the associated residual stress in the materials also relaxes very quickly in the beginning 30 hours. Therefore, it is low efficient to relax the residual stresses if prolonging the cooling stage more than 30 hours for the present experimental conditions. The calculation results have been proven by the H_2-bank Co., Ltd. in China, who chose the cooling time of 30 hours so that the fabrication of SOFCs is of high efficiency.

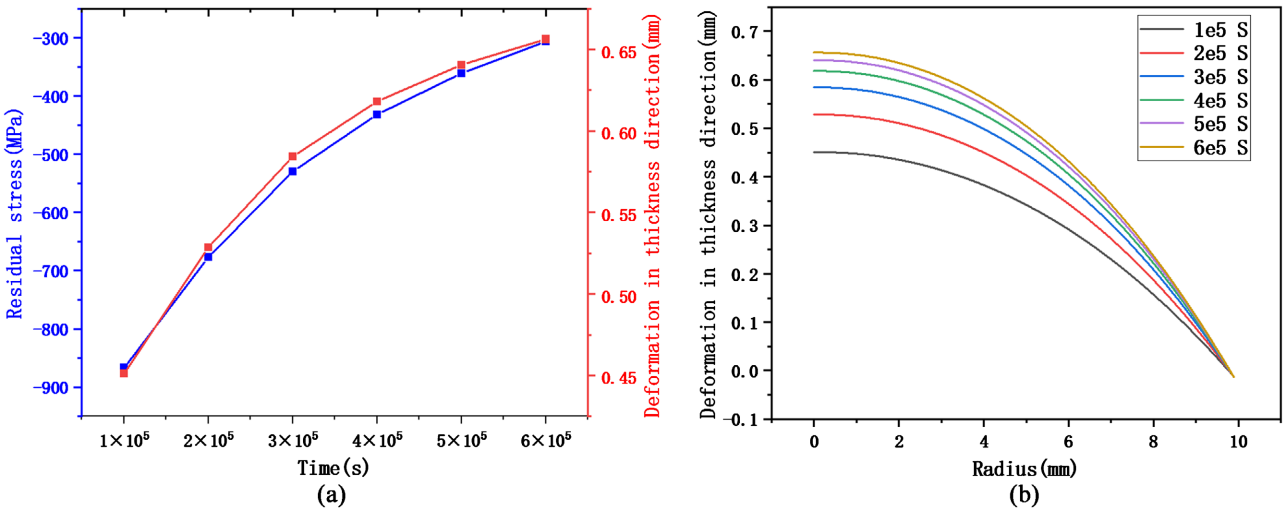

Figure 6. (a) The maximum residual stress, the maximum deformation in the thickness direction and (b) the deformation trend in the thickness direction change with the increase of cooling time.

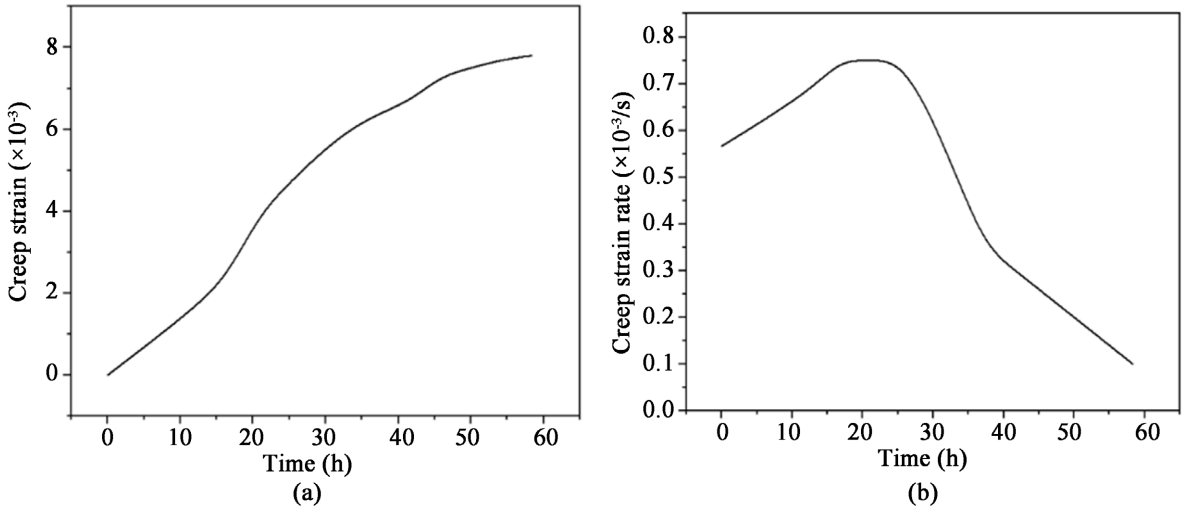

Figure 7. Relationship curves of (a) creep strain and (b) creep strain rate as a function of cooling time.

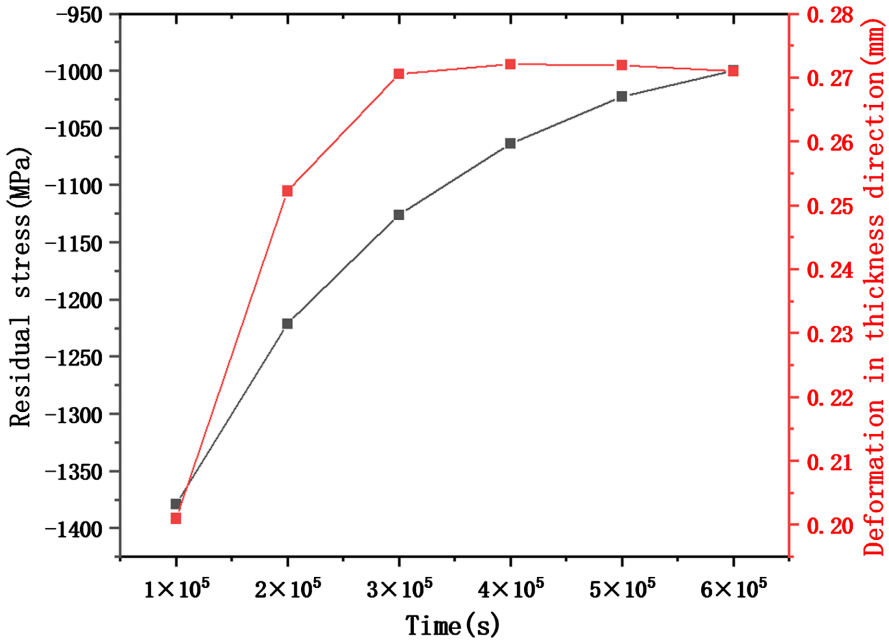

Figure 8. Effect of increasing cooling time on residual stress and thickness direction deformation of YSZ layer.

Therefore, the cooling time of the preparation process should be appropriately increased while the SOFC sample is pressurized. As shown in Figure 8, when the pressure was 0.13 MPa and the cooling time increased to 6×10^5 s (7 days), the overall stress-strain change of the sample tended to be stable, and the deformation remained stable at about 0.27 mm. The warping deformation is increased by 0.07 mm relative to the original sintering time, and the stress relaxation effect of residual stress due to creep decreases from −1379 MPa to −1000 MPa.

4. Discussion

Generally, the anode-supported cell was mechanical pressed by heavy ceramic

plates to avoid deformation during the co-firing at high temperatures. Otherwise, the warping in the SOFC cell will cause problems in the following screen-printing processing. In addition, the anode-supported cell with screen-printing functional layers was mechanically restricted, so that each single fabricated planar SOFC will be easily used for the fixation of the cells in the SOFC stack. However, that could induce large residual stresses in the thin functional layers. Generally, compressive stress is usually considered to be desirable because it is able to close the surface cracks improving the anti-fatigue properties. However, higher compressive stress can cause interfacial cracks or even cohesive failure (spallation). As the simulation results demonstrated, Moreover, compressive residual stress in the YSZ layer can be reduced at the sacrifice of increasing warping deformation. It is noted that both the warping morphography and residual stress in the functional layer at room temperature can be further reduced by optimizing the fabrication process. For example, the residual compressive stresses in the YSZ layer can be reduced by increasing the annealing time and adjusting the cooling time. Therefore, in order to make the SOFCs flat and have less residual stress, the cooling time of the preparation process should be appropriately increased while the SOFC sample is pressurized.

5. Conclusions

This study focused on the numerical investigation of residual stresses and warping in the planar SOFC. A 3D finite element model with the viscoelastic constitutive equations was established for calculating the residual stresses and warping of the cell. The main conclusions are summarized as follows.

1) A 3D finite element model using viscoelastic constitutive modeling was established for the simulation of cell fabrication at high temperatures.

2) Although the flat SOFC cells can be obtained by mechanical restriction during the high-temperature treatment, the concentration of compressive stress appears in the YSZ layer and may cause interfacial micro-cracks or even cohesive failure (spallation).

3) The residual stress of the YSZ layer in SOFC and the warpage deformation of the battery can be reduced by reducing mechanical constraint pressure and increasing creep time, and this cooling time history can be adjusted to improve the efficiency of the fabrication of SOFCs.

Conflicts of Interest

The authors declare no conflicts of interest regarding the publication of this paper.

References

[1] Yang, Z., Guo, M., Wang, N., Ma, C., Wang, J. and Han, M. (2017) A Short Review of Cathode Poisoning and Corrosion in Solid Oxide Fuel Cell. *International Journal of Hydrogen Energy*, **42**, 24948-24959. https://doi.org/10.1016/j.ijhydene.2017.08.057

[2] Kim, S.J., Choi, M.-B., Park, M., Kim, H., Son, J.-W., Lee, J.-H., Kim, B.-K., Lee, H.-W., Kim, S.-G. and Yoon, K.J. (2017) Acceleration Tests: Degradation of Anode-Supported Planar Solid Oxide Fuel Cells at Elevated Operating Temperatures. *Journal of Power Sources*, **360**, 284-293. https://doi.org/10.1016/j.jpowsour.2017.06.004

[3] Yakabe, H., Baba, Y., Sakurai, T. and Yoshitaka, Y. (2004) Evaluation of the Residual Stress for Anode-Supported SOFCs. *Journal of Power Sources*, **135**, 9-16. https://doi.org/10.1016/j.jpowsour.2003.11.049

[4] Lamas, J.S., Leroy, W.P. and Depla, D. (2014) Influence of the Target-Substrate Distance on the Growth of YSZ Thin Films. *Surface & Coatings Technology*, **241**, 26-29. https://doi.org/10.1016/j.surfcoat.2013.10.018

[5] Heenan, T.M.M., Robinson, J.B., Lu, X., Tjaden, B., Cervellino, A., Bailey, J.J., Brett, D.J.L. and Shearing, P.R. (2018) Understanding the Thermo-Mechanical Behaviour of Solid Oxide Fuel Cell Anodes Using Synchrotron X-Ray Diffraction. *Solid State Ionics*, **314**, 156-164. https://doi.org/10.1016/j.ssi.2017.10.025

[6] Malzbender, J., Fischer, W. and Steinbrech, R.W. (2008) Studies of Residual Stresses in Planar Solid Oxide Fuel Cells. *Journal of Power Sources*, **182**, 594-598. https://doi.org/10.1016/j.jpowsour.2008.04.035

[7] An, K., Clausen, B., Stoica, A.D., Armstrong, B.L., Skorpenske, H.D. and Wang, X.-L. (2010) *In-Situ* Neutron Diffraction Study of Phase Stress Evolutions in a Ni-Based Porous Anode Solid Oxide Fuel Cells under Uniaxial Load. *Applied Physics A*: *Materials Science & Processing*, **99**, 579-584. https://doi.org/10.1007/s00339-010-5629-9

[8] Frandsen, H.L., Chatzichristodoulou, C., Charlas, B., Kiebach, R., Kwok, K., Norby, P. and Hendriksen, P.V. (2021) Fast Relaxation of Stresses in Solid Oxide Cells through Reduction. Part I: Macro-Stresses in the Cell Layers. *International Journal of Hydrogen Energy*, **46**, 1548-1559. https://doi.org/10.1016/j.ijhydene.2020.10.145

[9] Dong, X., Zhang, C., Feng, X. and Hwang, K.C. (2013) Full-Field Measurement of Topography and Curvature by Coherent Gradient Sensing Method at High Temperature. *Experimental Mechanics*, **53**, 959-963. https://doi.org/10.1007/s11340-013-9713-x

[10] Lara-Curzio, E., Cakmak, E., Lin, L., Marquez-Rossy, A.E., Armstrong, B., Flores-Betancourt, A. and Macias, A. (2021) On the Nonlinear Temperature Dependence of Residual Stresses in Solid Oxide. *Fuel Cells*, **104**, 1014-1022. https://doi.org/10.1111/jace.17488

[11] Xie, J.-M. and Wang, F.-H. (2017) Thermal Stress Analysis of Solid Oxide Fuel Cell with Anode Functional Layer. *Journal of Inorganic Materials*, **32**, 400-406. https://doi.org/10.15541/jim20160341

[12] Zhao, X., Lu, Y., Song, X. and Wang, F. (2019) Evolution of the Residual Stress in Solid Oxide Fuel Cell during Creep. *Journal of the Australian Ceramic Society*, **55**, 681-687. https://doi.org/10.1007/s41779-018-0277-1

[13] Celik, S., Ibrahimoglu, B., Toros, S. and Mat, M.D. (2014) Three Dimensional Stress Analysis of Solid Oxide Fuel Cell Anode Micro Structure. *International Journal of Hydrogen Energy*, **39**, 19119-19131. https://doi.org/10.1016/j.ijhydene.2014.09.110

[14] Fang, X.R. and Lin, Z.J. (2018) Numerical Study on the Mechanical Stress and Mechanical Failure of Planar Solid Oxide Fuel Cell. *Applied Energy*, **229**, 63-68. https://doi.org/10.1016/j.apenergy.2018.07.077

[15] Molla, T.T., Kwok, K. and Frandsen, H.L. (2017) Transient Deformational Properties of High Temperature Alloys Used in Solid Oxide Fuel Cell Stacks. *Journal of*

Power Sources, **351**, 8-16. https://doi.org/10.1016/j.jpowsour.2017.03.059

[16] Zhang, Q., Xie, K., Luo, Y., Zhang, Y.-C. and Jiang, W.-C. (2022) Mismatch Effect of Material Creep Strength on Creep Damage and Failure Probability of Planar Solid Oxide Fuel Cell. *International Journal of Hydrogen Energy*, **47**, 2673-2684. https://doi.org/10.1016/j.ijhydene.2021.10.185

[17] Wu, Y.H., Xu, X.H., Yan, Z.L. and Zhong, Z. (2021) Thermo-Electro-Chemo-Mechanical Modeling of Solid Oxide Fuel Cell for Stress and Failure Evolution during Duty Cycle. *Journal of the Electrochemical Society*, **168**, Article ID: 044511. https://doi.org/10.1149/1945-7111/abf4ef

[18] Li, J., Kong, W. and Lin, Z. (2013) Theoretical Studies on the Electrochemical and Mechanical Properties and Microstructure Optimization of Micro-Tubular Solid Oxide Fuel Cells. *Journal of Power Sources*, **232**, 106-122. https://doi.org/10.1016/j.jpowsour.2013.01.006

[19] Muramatsu, M., Sato, M., Terada, K., Watanabe, S., Yashiro, K., Kawada, T., Iguchi, F. and Yokokawa, H. (2018) Shape Deformation Analysis of Anode-Supported Solid Oxide Fuel Cell by Electro-Chemo-Mechanical Simulation. *Solid State Ionics*, **319**, 194-202. https://doi.org/10.1016/j.ssi.2018.01.027

[20] Wang, Y., Jiang, W., Song, M., Zhang, Y. and Tu, S.-T. (2019) Effect of Frame Material on the Creep of Solid Oxide Fuel Cell. *International Journal of Hydrogen Energy*, **44**, 20323-20335. https://doi.org/10.1016/j.ijhydene.2019.05.220